IEEE Access
Multidisciplinary | Rapid Review | Open Access Journal

Received December 20, 2018, accepted February 8, 2019, date of publication February 21, 2019, date of current version March 20, 2019.

Digital Object Identifier 10.1109/ACCESS.2019.2900977

Analytical Analysis of SER for Beyond 5G Post-OFDM Waveforms in Presence of High Power Amplifiers

HMAIED SHAIEK[1], (Member, IEEE), RAFIK ZAYANI[1,2], (Member, IEEE), YAHIA MEDJAHDI[3], (Member, IEEE), AND DANIEL ROVIRAS[1], (Senior Member, IEEE)

[1]Conservatoire National des Arts et Métiers, 75003 Paris, France
[2]Innov'Com, Sup'Com, Carthage University, Ariana 2083, Tunisia
[3]Institut Supérieur d'Électronique de Paris, 75006 Paris, France

Corresponding author: Hmaied Shaiek (hmaied.shaiek@cnam.fr)

This work was supported by the framework of the WONG5 Project, through the French National Research Agency (ANR) under Grant ANR-15-CE25-0005.

ABSTRACT This paper studies the performance of enhanced multicarrier waveforms in the presence of a nonlinear memoryless high power amplifier (HPA). In particular, we focus on the in-band non-linear distortions (NLD) and their effects on symbol-error-rate. First, we introduce a theoretical characterization of NLD caused by HPAs. Two HPA models are considered in this paper: 1) a 4-GHz realistic HPA, modeled using a polynomial model, and this model exhibits both amplitude-to-amplitude (AM/AM) and amplitude-to-phase distortions and 2) a Rapp model, which exhibits only the AM/AM distortion. Second, we present further discussions and comparisons on the different waveforms: the cyclically prefixed orthogonal frequency division multiplexing (OFDM), the weighted overlap and add OFDM, the universal filtered multicarrier, the filtered OFDM, and the filter bank multicarrier based on offset-QAM. Then, we provide insights into the impact of in-band non-linear distortions caused by HPAs. The simulation and theoretical results are shown to be in agreement for different waveforms and various input back-off values.

INDEX TERMS 5G waveform, CP-OFDM, WOLA-OFDM, f-OFDM, UFMC, FBMC/OQAM, HPA, NLD, SER.

I. INTRODUCTION

5G is coming. Critical capability objectives to be fulfilled by international mobile telecommunication (IMT)-2020-compliant radio access include 20 Gbps peak data rate, 100 Mbps user experienced data rate, 10 $Mbps/m^2$ area traffic capacity, 10^6 devices/km^2 connection density, 1 ms latency and mobility up to 500 km/h [1] enhanced mobile broadband (eMBB), massive machine type communications (mMTC), and ultra-reliable and low latency communications (uRLLC) [2]. To meet these design goals, the third generation partnership project (3GPP) has launched the standardization activity for the first phase 5G system in Release 15 named New Radio (NR) in 2016, targeting deployment in 2018 and the ready system in 2020 [3]. In this regard, research, development and standardization activities for 5G wireless communication technologies has been ongoing in academia and international projects for several years. Examples of the key technologies considered include massive multiple-input multiple-output (MIMO), where the BSs are equipped with an excess of antennas to enhance both spectral-efficiency (SE) and energy-efficiency (EE) [4], enhanced multicarrier waveforms (MWF) flexibly accommodate various services/applications with different requirements [2], and so on.

Multicarrier waveforms have been consistently and fundamentally shaping the development of wireless communications. As the latest example, the cyclically prefixed orthogonal frequency division multiplexing (CP-OFDM) is largely adopted by physical layer (PHY) of today's long term evolution advanced (LTE-A). However, it is unlikely that 5G and Beyond challenges can be satisfied using CP-OFDM waveform. Indeed, the post-OFDM MWF chosen must allow for specific 5G asynchronous signaling scenarios, support large bandwidth (100 MHz and above), allow for high SE, support various multi-antenna techniques and flexible

The associate editor coordinating the review of this manuscript and approving it for publication was Julien Le Kernec.

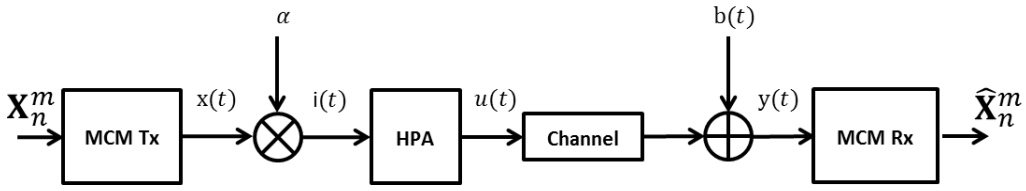

FIGURE 1. Basic MCM system model.

duplex, and allow for ultra-low latency, low-power and low-complexity design [2], [5].

A first class of these MWFs gathers the ones that adopt a per-subcarrier pulse-shaping to reduce out-of-band (OOB) emission and increase bandwidth efficiency and relaxed synchronization requirements: filter-bank multi-carrier based on offset QAM (FBMC/OQAM) [6]–[10] has been heavily studied. The universal filtered multicarrier (UFMC) [11] is another class of sub-band filtering based waveform, where only a transmit filter is used while the demodulation in the receiver relies on the oversampled discrete Fourier transform (DFT). Another filter based waveform is the filtered-OFDM (f-OFDM), firstly introduced in [6]. This multicarrier modulation bothers the classical CP-OFDM with sub-band filtering in order to improve the OOB radiation. Time-domain windowing can also be considered to achieve the desired enhancements, which is to prevent steep changes between two OFDM symbols so as to confine OOB emission. In this regard, an advanced windowing based waveform called - weighted overlap and add based OFDM (WOLA-OFDM) [11] has been studied. Interested readers are referred to [5] for an overview as well as qualitative and quantitative comparisons among different waveforms.

It is worth to mention some contributions related to the above mentioned MWFs. Zayani *et al.* [11] applied WOLA-OFDM in an asynchronous transmissions scenario. This MWF (WOLA-OFDM) has been shown to provide interesting performance with lower complexity compared to those based on filtering techniques [12]. Bouhadda *et al.* [13] studied the impact of in-band nonlinear distortions caused by memoryless HPA. The analysis carried in this study were restricted to CP-OFDM and FBMC/OQAM MWFs. Guan *et al.* [14] report a field in time division duplex down-link (TDD-DL) conducted on a configurable testbed in a real-world environment for the performance evaluations of CP-OFDM, Windowing-OFDM and f-OFDM.

Despite the mentioned MWFs advantages, they lose rapidly their good properties when non-linear (NL) radio frequency (RF) high power amplifiers (HPAs) are used, since they suffer from high Peak-to-Average Power Ratio (PAPR) of the modulated signal. In this regard and compared to the above contributions, this paper presents an analytical study of the effect of memoryless power amplifiers on the performance of the most promising post-OFDM MWFs. In particular, we focus on the in-band non-linear distortions (NLD) and their effects on system symbol error rate (SER) performance.

The main contributions of this paper are: we focus our attention firstly on developing a universal approach to make this study feasible for any measured or modeled memoryless HPA model and for each MWF. Results using analytical expressions can be served to validate the ones obtained by simulations. We present further discussions and comparisons on different waveforms: CP-OFDM, WOLA-OFDM, UFMC, f-OFDM and FBMC/OQAM and we provide insights on the impact of in-band NLD caused by RF HPA.

The rest of this present paper is structured as follows. Section II describes the considered system model. In particular, the detailed principle of CP-OFDM, WOLA-OFDM, UFMC, f-OFDM and FBMC/OQAM and the considered HPA models are presented, respectively. In section III, the approach to characterize theoretically NL HPA distortions is presented. In section IV, parameter selections are defined and waveform performances are validated and compared via both simulations and analytical models. The relevant performance, in terms of SER, are discussed. Finally, the conclusion is given in section V.

Notations : $\mathbb{E}[.]$ stands for the expectation operator and $(.)^*$ denotes the complex conjugate operation.

II. SYSTEM MODEL

Fig. 1, shows a generic transmission scheme MWFs in presence NL HPA. The Multi-Carrier-Modulation (MCM) block modulates the signal by one of the MWFs selected in this paper : CP-OFDM, WOLA-OFDM, UFMC and f-OFDM. The signal: $x(t)$ at the output of MCM block is than weighted be a scalar gain α in order to have a signal $i(t)$ with a given Input Back-Off (IBO), at the input of the HPA. Depending on the HPA NLD, the amplified signal will suffer from in band distortions as well as out off band distortions. We underline that in this paper, only in band distortions will be studied. After propagation over a given channel, the received signal will be demodulated and the channel equalized, if required, before achieving symbols decision. In the next section, we will give short description of the MWFs considered in this paper, along with the two HPAs models.

A. SELECTED WAVEFORMS

1) CP-OFDM

The CP-OFDM transmitter and receiver are implemented using the inverse fast Fourier transform (IFFT) and FFT, respectively. In order to keep the orthogonality between

subcarriers, a cyclic prefix (CP) is usually inserted transforming thus the linear channel convolution into circular convolution if the CP is longer than channel impulse response. Therefore, after the FFT operation, the channel equalization becomes trivial through a single coefficient per subcarrier.

2) WOLA-OFDM

This MWF introduces a time-domain window to control the OOB emission. The WOLA-OFDM [15] has been intensively discussed along this line of study, and schemes have been proposed for asynchronous 5G [11], [12]. The boundaries of each CP-OFDM symbol are multiplied with a smooth window in time-domain (e.g, a window, a Hanning window). The increasing window is applied at the beginning of the CP while the decreasing window is applied on a cyclic suffix (CS), corresponding to the first W_{Tx} samples added at the end of the OFDM symbol (see. Fig. 4). Thus, the WOLA-OFDM time domain symbol is cyclically extended from N samples to $+CP+W_{Tx}$. In order to achieve the same spectral efficiency as CP-OFDM, WOLA-OFDM symbols are overlapping.

At WOLA-OFDM receiver, an advanced windowing is also applied in order to enhance asynchronous inter-user interference suppression [11]. The applied receive window is independent from the one applied at the transmitter and its length is equal to $N + 2W_{Rx}$.

3) UFMC

The key design feature of UFMC is the resource block (RB)-wise filtering operation [16]–[18], which is implemented by utilizing finite impulse response (FIR) filters. Indeed, each RB is filtered by the corresponding FIR filter after the inverse discrete Fourier transform (IDFT) and the zero padding (ZP) operation.[1] Note that this RB-wise filtering leads to a shorter FIR compared to the per-subcarrier filtering approach. Such a property improves the UFMC suitability to short-packet transmission context. In order to recover the transmitted data, a basic ZP-OFDM receiver is used with additional processing (e.g. windowing) in the case of multi-user interference context.

4) F-OFDM

Similar to UFMC, f-OFDM was proposed in [6] by combining the classical CP-OFDM with subband-wise filtering which brings an improvement in terms of spectral localization. In order to mitigate the interference caused by time and/or frequency misalignment, a similar filter is used at the receiver side before the basic CP-OFDM demodulator. Note that f-OFDM suffers from inter-block interference because the FIR length is allowed to exceed the CP [19]. However, the impact of this interference can be reduced by designing properly the filter. Moreover, a truncation is applied at the burst edges in order to make f-OFDM well localized in the time domain. Unfortunately, such a procedure will impact the frequency localization of f-OFDM. However, the results in [19] show that, truncating the burst by half CP length on each side, presents a good compromise between the short packet requirement and the frequency localization.

[1] It is used to absorb the filter transient response

5) FBMC/OQAM

FBMC/OQAM is a per-subcarrier filtering-based waveform using well-localized prototype filters. Such a key property provides the capability of using fragmented spectrum with a relaxed synchronization. However, this advantage is at the price of the orthogonality condition that is restricted to the real domain by using the OQAM modulation where the in-phase and the quadrature components of the input data symbols are time staggered by half a symbol period [20], [21].

B. HPAs MODELS

Broadly, the nonlinear HPA models can be classified to two categories; memoryless nonlinear models and nonlinear models with memory. The memoryless characterize the power dependent nonlinear behavior by AM/AM (amplitude to amplitude modulation) and AM/PM (amplitude to phase modulation) conversion characteristics. Nonlinear models with memory aim also to capture the effects that are manifested not only by the instantaneous input signal magnitude but also the frequency dependent characteristics of the signal envelope e.g. making AM/AM and AM/PM functions non-static and depend on the past input levels. Memory effects in HPAs are attributed to various sources, thermal and electric [22], [23]. These effects are more elevated in high HPAs, but also appear as the signal bandwidth is increased.

This nonlinearity phenomena leads to in-band performance degradation and spectral regrowth causing adjacent channel interference. For in-band signal these distortions are quantified by Symbol Error Rate (SER) at the receiver. HPA nonlinearities have especially noticeable impacts on small devices and thus for especially important for UL transmission but for higher mmWave frequencies HPA could also impact and set constraints to DL transmission. The dynamic long term memory effects in PA introduce asymmetry in sidebands Adjacent Channel Leakage Ratio (ACLR) or Intermodulation Distortion (IMD) variation due to envelope frequency [22]–[24].

Volterra series are well-known method to model nonlinear systems with memory accurately. The main drawback of it is the high complexity of the model. One common derivative of Volterra series is Memory Polynomial (MP) model [25], [26], providing good modeling accuracy with somewhat reduced complexity. MP model (and other derivatives of Volterra series) have widely been used in predistortion studies of wide-band high PA. Other common industry adopted approach is to use the memoryless nonlinear model through AM/AM and AM/PM conversion characteristics. This approach, while not necessarily capturing the possible asymmetry, offers reasonable accuracy and merits in simulation simplicity. Furthermore, memoryless models have been used extensively in the academic studies as well as many earlier evaluations carried out in RAN4 and related studies [27].

Therefore, it is felt that for initial evaluations of post-OFDM waveform, one could choose memoryless nonlinear measured or modeled HPA as those considered in [27]. MP type models could be considered further on later studies to fine tune the 5G and Beyond systems requirements.

In practice, in order to avoid or at least to reduce the effects of nonlinearities, the HPA is operated at a given Input Back-Off (IBO) from its $1dB$ compression point [28]. The $1dB$ compression point refers to the input power level where the transfer characteristics of the amplifier have dropped by 1 dB from the ideal linear characteristics.

In the log scale, the signal IBO is defined as follows:

$$\mathrm{IBO} = 10\log_{10}\left(\frac{P_{1\mathrm{dB}}}{P_i}\right) \tag{1}$$

where P_{1dB} is the input power at the $1dB$ compression point and P_i is the mean power of the input signal.

As illustrated in Fig. 1, before amplifying the signal $x(t)$, by the HPA, it is necessary to scale it by a real positive gain α to ensure a given IBO. For a given mean power: $P_x = \mathbb{E}\left[|x(t)|^2\right]$, of the signal $x(t)$, the gain α needed to ensure a signal $i(t)$, with a given IBO value is:

$$\alpha = \sqrt{\frac{P_{1\mathrm{dB}}}{10^{\frac{IBO}{10}} P_{\mathrm{x}}}} \tag{2}$$

The complex envelope $i(t)$ of the signal at the input of the HPA can be written as:

$$i(t) = \rho(t)e^{j\varphi(t)} \tag{3}$$

where:

- $\rho(t)$ is the input signal modulus, and
- $\varphi(t)$ is the input signal phase.

In practice, the HPA cannot be considered as a linear device. Then, as a general formulation, the amplified signal $u(t)$ can be written as:

$$u(t) = F_a(\rho(t))e^{j(F_p(\rho(t))+\varphi(t))} \tag{4}$$

where:

- $F_a(\rho(t))$ is the AM/AM characteristic of the HPA,
- $F_p(\rho(t))$ is the AM/PM characteristic of the HPA.

We can rewrite Eq. (4) as following:

$$u(t) = S(\rho(t))e^{j\varphi(t)} \tag{5}$$

where $S(\rho(t)) = F_a(\rho(t))e^{jF_p(\rho(t))}$ is the complex soft envelope of the amplified signal $u(t)$.

The AM/AM and AM/PM characteristics cause distortions on the signal constellation in addition to spectral regrowth, degrading then the system performance. For purpose of theoretical studies, it is necessary, for a given HPA, to propose a mathematical model to reproduce or approximate its NL effects in amplitude (AM/AM) and phase (AM/PM) [29], [30]. In the literature, two main families of HPA models can be found: the memoryless HPA models and the HPA models with memory. In this study, we will assume that the HPA frequency response is constant over the useful signal frequency band, which allows neglecting the memory effects of the HPA. Thus, any change in the signal input occurs instantaneously at the output.

Many memoryless HPA models have been proposed and studied in literature. Among them we can cite :

- The Soft Envelop Limiter (SEL), used for modeling a HPA with a perfect predistortion system,
- The Rapp model, commonly used for modeling Solid State Power Amplifiers (SSPA) [31],
- The Saleh model, generally used for modeling Travelling Wave Tube Amplifiers (TWTA) [32],
- The polynomial model, widely used for purpose of theoretical analysis of NL HPA effects.

In the following paragraphs, a brief description will be given for the two HPA models considered in this paper.

1) HPA1: POLYNOMIAL MODEL

This model is based on a measured commercial 4 GHz long term evolution (LTE) user equipment HPA provided by [33], exhibiting both AM/AM and AM/PM distortions. The measured AM/AM and AM/PM curves of this HPA model are approximated using a full rank polynomial model with order $P = 9$. The signal $u(t)$ at the output of the HPA device can be written:

$$u(t) = \sum_{l=1}^{P} a_l \rho(t)\,|\rho(t)|^{l-1} \tag{6}$$

where a_l are the complex coefficients of the polynomial approximation, computed by using a classical Least Square (LS) method.

By combining Eq. (4) and Eq. (6), we can write the complex soft envelope of the signal $u(t)$ as:

$$S(\rho(t)) = F_a(\rho(t))e^{jF_p(\rho(t))} = \sum_{l=1}^{P} a_l \rho(t)^n \tag{7}$$

2) HPA2: MODIFIED RAPP MODEL

For HPA2, based on a modified Rapp model, the amplified signal exhibits only amplitude distortion. The AM/AM conversion function: $F_a(\cdot)$, of the modified Rapp model can be expressed as follows:

$$F_a(\rho(t)) = \frac{G_0\rho(t)}{\left(1 + \left|\frac{G_0\rho(t)}{A_{sat}}\right|^{2p}\right)^{\frac{1}{2p}}} \tag{8}$$

where G_0 is the linear gain, A_{sat} is the saturation voltage and p a smoothness factor that controls the transition from the linear region to the saturation region, ($p > 0$). For purpose of theoretical analysis of HPA2 effects on transmitted signals, the AM/AM characteristic of this HPA model will be approximated with a polynomial model.

The AM/AM conversion characteristics of the two HPA models are given by Fig. 2. In this figure, we remind that the order of the polynomial approximation used for HPA1 is equal to 9.

As expected from a Rapp model, HPA2 AM/AM conversion characteristic shows a linear performance for low amplitudes of the input signal. Then, a transition towards a constant

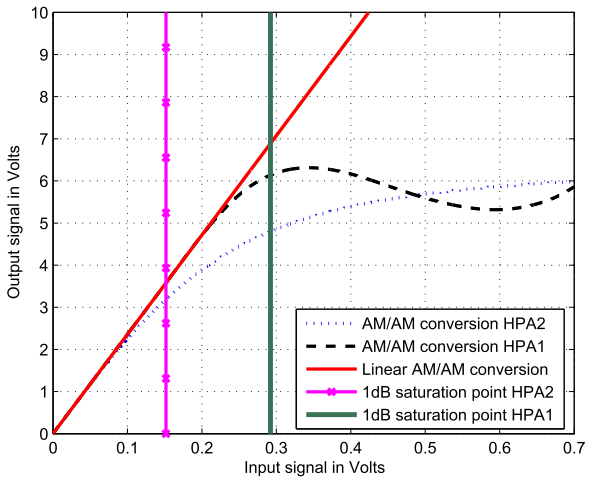

FIGURE 2. AM/AM conversion characteristics of HPA1 and HPA2.

saturated output is observed. When $p \to \infty$, the Rapp model converges towards the SEL one. The parameters G_0 and A_{sat}, are computed to make the linear gain of this HPA model equal to that of HPA1. The knee factor p is chosen to be equal to 1.1 to have a different compression point from that of HPA2 model.

The AM/PM conversion characteristics of the HPA1 is given by Fig. 3.

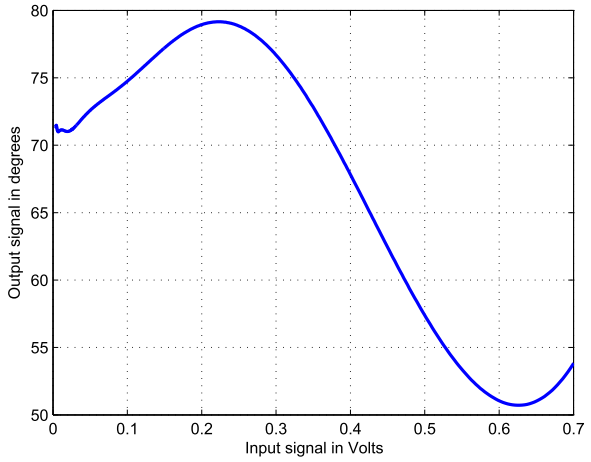

FIGURE 3. HPA1 model: AM/PM conversion.

In the next section we will develop theoretical analysis to evaluate the impact of the HPA models, described in this section, on the considered waveforms SER over Additive White Gaussian Noise (AWGN) channels.

III. THEORETICAL ANALYSIS OF SER PERFORMANCE

A. NON LINEAR DISTORTION MODELING

A theoretical characterization of NLD effects on CP-OFDM systems has been proposed in [34], where the authors focused on the impact of the NL distortions induced by three HPA models: the SEL, the SSPA, and the TWTA. We note that, except for the SEL HPA model, the investigation presented in [34] gives only semi-analytical results which could not be easily extended to real HPA with measured characteristics, which is the case of one of the HPA models (HPA1) considered in this paper. Other contributions [35], [36] used the results presented in [34] to study the effect of HPA on Multiple-Input Multiple-Output (MIMO) transmit diversity systems. Bouhadda *et al.* [13] proposed a theoretical characterization of the NLD parameters for any measured or modeled HPA. The results presented in [13], were limited to CP-OFDM and FBMC/OQAM waveforms.

One of the main contribution of this study is to investigate the in-band impact (SER) of a real-life and a modeled HPAs over the selected post-OFDM MWFs. The analysis carried in this paper are based on the theoretical NLD parameters characterization proposed in [13].

The SER performance analysis, proposed in this paper is based on Bussgang theorem [37], saying that if the input HPA signal $i(t)$ has a Gaussian (which's true for all the MWFs considered in this paper, when the number of subcarriers N is large) distribution, the HPA output signal $u(t)$ can be expressed as:

$$u(t) = K_0 i(t) + d(t) \tag{9}$$

where:

- $d(t)$ is a zero mean noise, which is uncorrelated with $i(t)$:
- K_0 is a complex gain with modulus $|K_0|$ and phase ϕ_{K_0}.

For simplicity sake, we will discard, in the following equations, the time variable t, from ρ and φ. According to [34], K_0 can be computed analytically by:

$$K_0 = \frac{1}{2}\mathbb{E}\left[\frac{\partial S(\rho)}{\partial \rho} + \frac{S(\rho)}{\rho}\right] \tag{10}$$

We recall that $S(\rho) = F_a(\rho)e^{jF_p(\rho)}$ is the complex soft envelop of the signal $u(t)$, at the output of the HPA.

The variance σ_d^2 of the NLD noise $d(t)$ is given by:

$$\sigma_d^2 = \mathbb{E}(|d(t)|^2) = \mathbb{E}\left(|S(\rho)|^2\right) - |K_0|^2\,\mathbb{E}(\rho^2). \tag{11}$$

In [13], an attractive approach, for computing the NLD parameters K_0 and σ_d^2, has been proposed. For a given modeled or measured HPA, this approach is based on polynomial modeling of the HPA conversion characteristics (Eq. (6)), followed by the computation of the expectation of ρ^l (with l a positive integer).

The authors would like to recall, here, the analytical expression for computing the NLD parameters K_0 and σ_d^2. Indeed, the authors have checked Eq. (32) and Eq. (33) in paper [13] and fixed some errors, leading to the following updated expression for computing the complex gain K_0:

$$K_0 = a_1 + \sqrt{\frac{\pi}{8}} \sum_{l=2,leven}^{P} (l+1)a_l \sigma^{l-1} \prod_{i=0}^{\frac{l-2}{2}} (2i+1) + \frac{1}{2} \sum_{l=3,lodd}^{P} (l+1)a_l (\sqrt{2}\sigma)^{l-1} \left(\frac{l-1}{2}\right)! \tag{12}$$

where:

- $\sigma = \sqrt{P_i} = \sqrt{\alpha^2 P_x} = \sqrt{\frac{P_{1dB}}{10^{\frac{IBO}{10}}}}$ is the standard deviation of the HPA input signal,
- ! stands for the factorial operator.

For the variance σ_d^2 of the NLD noise $d(t)$. The updated expression is given by:

$$\sigma_d^2 = \sum_{l=1}^{P} |a_l|^2 2^l \sigma^{2l} l! - 2|K_0|^2 \sigma^2 + \sqrt{\frac{4\pi}{2}} \sum_{l,n=1, l\neq n, (l+n)odd}^{P} \Re[a_l a_n^*] \sigma^{l+n} \prod_{i=0}^{\frac{l+n-1}{2}} (2i+1) + 2 \sum_{l,n=1, l\neq n, (l+n)even}^{P} \Re[a_l a_n^*] (\sqrt{2}\sigma)^{l+n} (\frac{l+n}{2})! \quad (13)$$

where $\Re[.]$ stands for the real part.

B. SER THEORETICAL ANALYSIS OF MWFs OVER AWGN CHANNEL

According to Eq. (9) and the system model shown in Fig. 1, we can write the received signal $y(t)$, in presence of AWGN channel as follows:

$$\begin{aligned} y(t) &= u(t) + b(t) \\ &= K_0 i(t) + (d(t) + b(t)) \\ &= K_0 \alpha x(t) + (d(t) + b(t)) \end{aligned} \quad (14)$$

We assume a perfect compensation for the complex gain K_0 at the receiver side. This compensation can be jointly made with the channel estimation process. After compensation for the multiplicative gain K_0, it is straightforward to write, that, over AWGN channel, the SER of M-QAM modulated symbols with an MCM scheme [38], as:

$$SER(E_b/N_0) = 2(1 - \frac{1}{\sqrt{M}}) \times erfc\left(\sqrt{\frac{3\alpha^2 log_2(M)}{2(M-1)P_n}}\right) \quad (15)$$

where:

- $P_n = (\sigma_d^2 + \sigma_b^2)/|K_0|^2$ is the total power of both non-linear noise $d(t)$ and thermal one $b(t)$,
- $\sigma_b^2 = P_u/(log_2(M).E_b/N_0)$ is the thermal noise variance corresponding to E_b/N_0,
- M is the size of QAM constellation.

From Eq. (2), it is obvious that the *IBO* coefficient α depends on the considered MCM scheme. Indeed, the average power of the transmitted signal $x(t)$: P_x can be influenced by the windowing and/or the filtering processes used in the MCM transceiver. This is a key point of the analysis carried out in next sections.

1) CP-OFDM

Let P_0 be the CP-OFDM per-sample average power. Since there is no windowing nor filtering, we can write the mean power of a CP-OFDM symbol ($P_x^{CP-OFDM}$) as:

$$P_x^{CP-OFDM} = (N + CP)P_0 \quad (16)$$

2) WOLA-OFDM CASE

For WOLA-OFDM, we have a signal with a constant mean power on each sample except at the beginning and at the end of the symbol. As illustrated in Fig. 4, every $CP + N + W_{Tx}$ samples we have a diminution of the per-sample average power due to the applied windowing process. Finally, we get the WOLA-OFDM signal represented in Fig. 5.

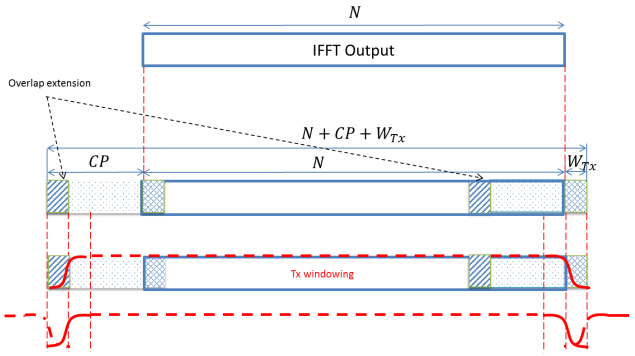

FIGURE 4. WOLA-OFDM transmitted signal.

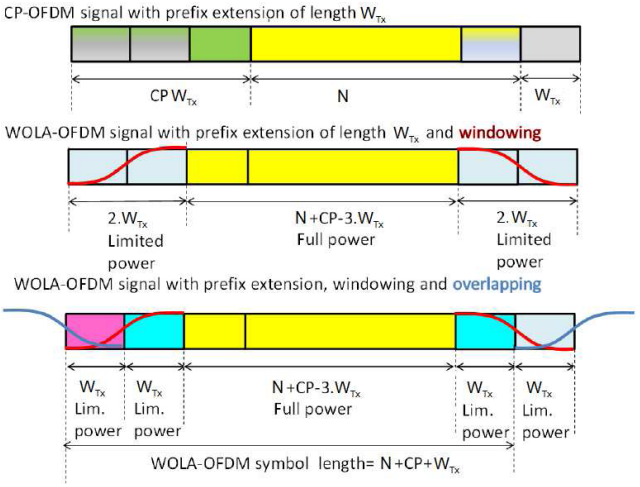

FIGURE 5. WOLA-OFDM signal power.

The mean power of a given WOLA-OFDM (of length $N + CP$) symbol $P_x^{WOLA-OFDM}$ is equal to:

$$P_x^{WOLA-OFDM} = P_0(N + CP - 3.W_{Tx}) + 2P_0 \sum_{k=1}^{W_{Tx}} \omega_{Tx}^2(k) + 2P_0 \sum_{k=W_{Tx}+1}^{2W_{Tx}} \omega_{Tx}^2(k) \quad (17)$$

The overlapping between successive WOLA-OFDM symbols has been taken into account through the coefficient 2 in the last two terms of Eq. (17).

Since $\omega_{Tx}(k) \leq 1$, the mean power of a WOLA-OFDM symbol $P_x^{WOLA-OFDM}$ is lower than the one of CP-OFDM

$P_x^{CP-OFDM}$. Then, the WOLA-OFDM signal has to be amplified in order to have an equivalent IBO equal to that of CP-OFDM. For the crests of the WOLA-OFDM signal, this is equivalent to having an equivalent lower IBO.

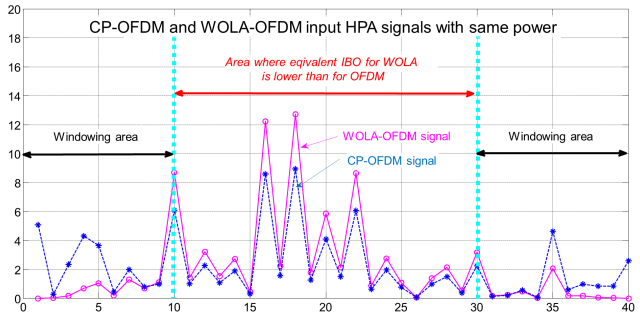

FIGURE 6. Equivalent IBO illustration.

In Fig. 6, we have plotted a CP-OFDM and a WOLA-OFDM signals with $N = 40$ and $W_{Tx} = 10$. The two signals have the same power and, then, they correspond to the same IBO. Nevertheless, looking at WOLA-OFDM signal in the middle region, it's clear that this signal has different IBO than the CP-OFDM one (dashed star one). This different IBO, named in the following as "equivalent IBO" and noted IBO_{equ}^{MCM} for a given MCM scheme, will be taken into account for computing the SER. In fact, for WOLA-OFDM, the major part of the signal at the HPA input will be seen with an "equivalent IBO". In the computation of SER, given by Eq. 15, P_n and α must be computed with this equivalent IBO.

To this end, the gain that has to be applied to the WOLA-OFDM time domain signal can be calculated as follows:

$$\Delta_G^{WOLA-OFDM} = \frac{P_x^{CP-OFDM}}{P_x^{WOLA-OFDM}} \tag{18}$$

This extra gain corresponds to a loss in terms of IBO for WOLA-OFDM:

$$IBO_{equ}^{WOLA-OFDM} = IBO^{CP-OFDM} - 10log10(\Delta_G^{WOLA-OFDM}) \tag{19}$$

The theoretical SER for WOLA-OFDM has to be computed with Eq. (15) using updated coefficients K_0 and σ_d^2 that are computed for the equivalent $IBO_{WOLA-OFDM}$ given by Eq. (19).

3) UFMC CASE

Similar to WOLA-OFDM, the UFMC signal has a constant mean power on each sample except at the beginning and at the end of the UFMC block. In fact, we have a reduction of the per-sample average power due to the filtering applied at the transmitter side. As illustrated in Fig. 7, we distinguish three areas within every UFMC block of $N + CP$ samples:

- Ramp-up area: from time domain sample $k = 0 : L_u - 1$ (first part of the UFMC symbol),

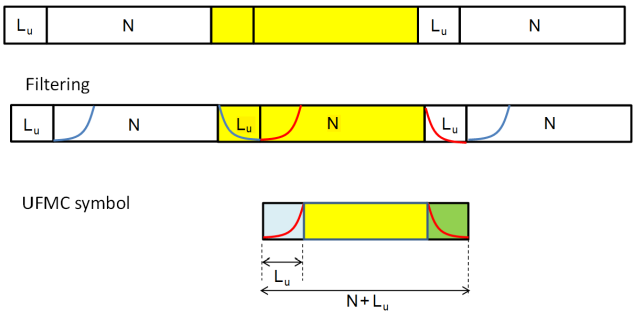

FIGURE 7. UFMC transmitted signal.

- Constant power area: from time domain sample $k = L_u$: $L_u + N - 1$ (middle part of the UFMC symbol),
- Ramp down area: from time domain sample $k = L_u + N$: $L_u + N + L_u - 1$ (last part of the UFMC symbol).

where L_u is the FIR length.

Let $[s(0), s(1), \ldots, s(N-1)]$ be the N OFDM time domain samples, after filtering we get $[c(0), c(1), c(2), \ldots, c(N-1+L_u)]$ non zero samples,

1) $c(0) = h(0)s(0)$
2) $c(1) = h(0)s(1) + h(1)s(0)$
3) $c(2) = h(0)s(2) + h(1)s(1) + h(2)s(0)$
4) $c(n) = \sum_{k=0}^{L_u-1} h(k)s(n-k)$
5) $\mathbb{E}(c(n)c(n)^*) = \sum_{k=0}^{n} |h(k)|^2.E(|s(n-k)|^2) = \sum_{k=0}^{n} |h(k)|^2).P_0$

where $P_0 = E(|s(n)|^2)$ is the mean power of a time domain sample and $h(k)$ is the k^{th} coefficient of the FIR of the transmit filter.

Therefore, the per-sample average power can be written as follows

- Ramp-up area:

$$\mathbb{E}(|c(n)|^2) = \sum_{k=0}^{n} |h(k)|^2 P_0$$

- Constant power area:

$$\mathbb{E}(|c(n)|^2) = \sum_{k=0}^{L_u-1} |h(k)|^2 P_0$$

- Ramp down area:

$$\mathbb{E}(|c(n)|^2) = \sum_{k=n-N-CP-L_u}^{L_u-1} |h(k)|^2 P_0$$

Considering the three areas, the UFMC symbol mean power can be written as:

$$P_x^{UFMC} = P_0[(N + CP + 3.L_u) \sum_{k=0}^{L_u-1} h(k)^2 + 2 \sum_{k=0}^{L_u-1} (L_u - k)h(k)^2] \tag{20}$$

Accordingly, the UFMC symbol mean power is then lower than the one of CP-OFDM. As for the WOLA-OFDM case, the UFMC signal has to be amplified in order to have the same IBO as CP-OFDM. In order to do so, the gain that has to be applied to the UFMC time domain signal is equal to:

$$\Delta_G^{UFMC} = \frac{P_x^{CP-OFDM}}{P_x^{UFMC}} \tag{21}$$

This extra gain corresponds to an equivalent IBO for UFMC given by:

$$IBO_{equ}^{UFMC} = IBO^{CP-OFDM} - 10log10(\Delta_G^{UFMC}) \tag{22}$$

4) F-OFDM CASE

As for WOLA-OFDM and UFMC, the f-OFDM signal has a constant mean power on each time domain sample except at the beginning and at the end of the frame of K OFDM blocks. We have thus a diminution of per-sample average power due to the filtering process. Note that for very long frames ($K >> 1$), the performance of f-OFDM will be close to that of CP-OFDM one since the filter ramp up/down length is negligible with respect to the $K \times (N + CP)$. However, the f-OFDM SER performance will be detrimentally impacted in the case of short frames. For instance, the construction of a single f-OFDM frame with $K = 2$ is illustrated in Fig. 8.

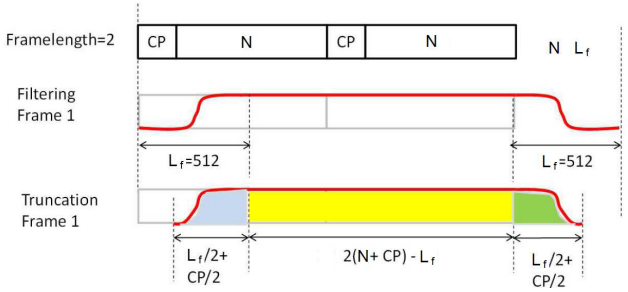

FIGURE 8. f-OFDM symbol.

After the truncation and similar to UFMC, we have three regions within a f-OFDM frame:

- Truncated ramp-up area: from time domain samples $k = 0 : L_f/2 + CP/2 - 1$ (first part of the symbol),
- Constant power area: from time domain sample $k = L_f/2 + CP/2 : L_f/2 + CP/2 + K(N + CP) - L_f$ (middle part of the symbol),
- Truncated ramp down area: from time domain samples $k = K(N + CP) + CP - L_f/2 - CP/2 : K(N + CP) + CP$ (last part of the symbol).

where L_f is FIR filter length.

Since the impulse response of the filter is symmetrical, the per-sample average power in the ramp-up region is identical to the ramp-down one. Consequently, the per-sample average power can be written as:

- Ramp-up/down area:

$$\mathbb{E}(|c(n)|^2) = \sum_{k=n}^{L_f-1} |h(k)|^2 P_0$$

- Constant power area:

$$\mathbb{E}(|c(n)|^2) = \sum_{k=0}^{L_f-1} |h(k)|^2 P_0 \tag{23}$$

where $h(k)$ is the k^{th} coefficient of f-OFDM sub-band filter

Finally, the mean power of an f-OFDM frame becomes:

$$P_x^{f-OFDM} = P_0.[\sum_{k=n}^{L_f-1} |h(k)|^2 (K(N + CP)L_f) + 2(\sum_{n=0}^{L_f/2+CP/2-1} \sum_{k=n}^{LV-1} |h(k)|^2)] \tag{24}$$

The gain that has to be applied to the f-OFDM time domain signal is equal to:

$$\Delta_G^{f-OFDM} = \frac{P_x^{f-OFDM}}{P_x^{CP-OFDM}} \tag{25}$$

This extra gain corresponds to an equivalent IBO for f-OFDM given by:

$$IBO_{equ}^{f-OFDM} = IBO^{CP-OFDM} - 10log10(\Delta_G^{f-OFDM}) \tag{26}$$

IV. NUMERICAL RESULTS

Theoretical study introduced in previous section were performed in order to evaluate the performance of studied multicarrier waveforms in presence of nonlinear HPA. They are built around a system setup that, first, identifies a behavioral model of the PA using polynomial model, and then validates it by comparing simulated results and the theoretical ones.

A. SYSTEM SETUP

We recall that two HPA models are considered in this work. The first one (HPA1) is a 4 GHz realistic one [33]. With this HPA1 model we have AM/AM distortion together with AM/PM distortion. The second HPA (HPA2) model is a Rapp modified model, which linear gain has been adjusted to be equal to that HPA1. With HPA2 model we have only AM/AM distortion. A brief summary of system setup and parameters is provided in Table 1.

B. COMPARISON BETWEEN THEORETICAL AND SIMULATED SER PERFORMANCE

It is worth noticing that FBMC/OQAM has similar performances as the classical CP-OFDM for different IBOs and HPAs. This behavior can be explained by the fact that this two WFs have the same mean power for each symbol. The SER given by Eq. 15 is thus computed by using the same equivalent IBO as that of CP-OFDM (equal to the real IBO in this case).

Concerning WOLA-OFDM, UFMC and f-OFDM, we note some performance degradations compared to CP-OFDM. This is related to the different structures of these post-OFDM waveforms.

TABLE 1. Scenario parameters.

General parameters	
FFT size (N)	1024
Input data (M)	16-QAM, 64-QAM
WF1: CP-OFDM / WF2: WOLA-OFDM	
CP length (CP)	72
Windowing	Meyer Raised cosine
Window length (W_{Tx},W_{Rx})	(20, 32)
WF3: UFMC	
Filter	Dolph-Chebyshev
Filter length (L_u =CP+1)	73
Zero padding length	72
Stop-band attenuation	40 dB
Receive windowing	Raised cosine
WF4: f-OFDM	
Filter	the same at both Tx and Rx sides
Filter length (L_f)	512
CP length	72
Burst truncation	CP/2 on each side
WF5: FBMC/OQAM	
Prototype Filter	PHYDYAS
Overlapping factor (K)	4

1) WOLA-OFDM CASE

Fig. 9 presents the SER of WOLA-OFDM for $N = 1024$, $CP = 72$, $W_{Tx} = W_{Rx} = 20$, 64-QAM and for HPA2 with three IBOs= 2, 3 and 4dB. We can see that there is a very good match between theoretical and simulation results.

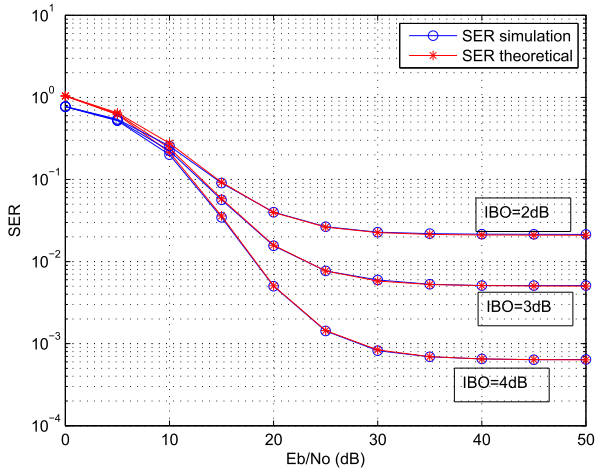

FIGURE 9. WOLA-OFDM performance for different IBOs for HPA2.

Fig. 10 presents the SER of WOLA-OFDM for $N = 1024$, $CP = 256$, 64-QAM, HPA2 with $IBO = 4dB$ and various values of W_{Tx}. When W_{Tx} is increasing, the length of the modulated signal holes increases, yielding a lower equivalent IBO and thus a lower SER performance. We can see on Fig. 10 that, again, there is a good match between theoretical and simulation results.

2) UFMC CASE

The theoretical SER for UFMC has the same expression as the SER of CP-OFDM except that coefficients K_0 and σ_d^2 are computed for the equivalent IBO_{equ}^{UFMC} given by Eq.(22).

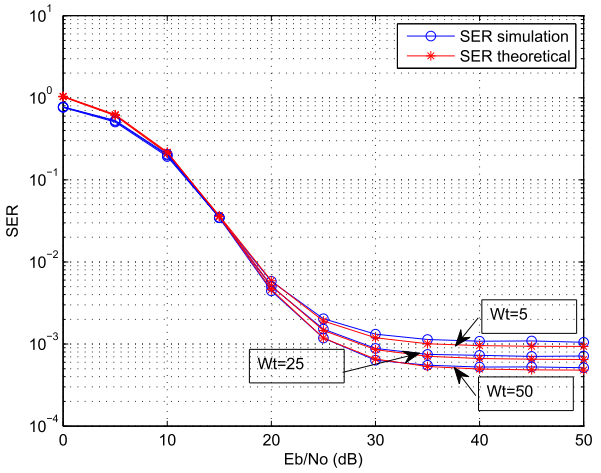

FIGURE 10. WOLA-OFDM performance for different values of W_{Tx}, HPA2, IBO = 4dB, N = 1024, CP = 256, W_{Tx} = [50, 25, 5].

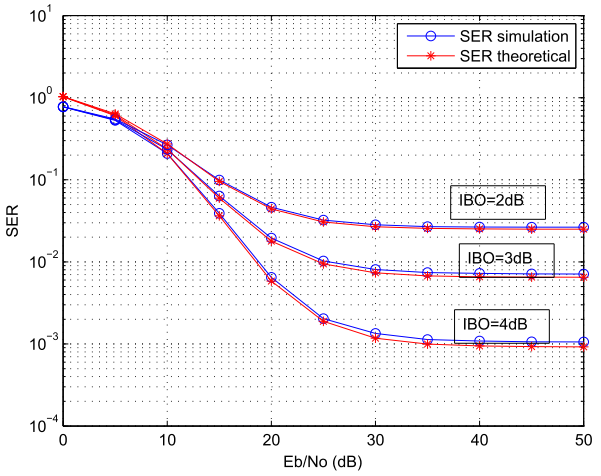

FIGURE 11. UFMC performance for HPA2 and IBO = 4, 3, 2dB.

Fig. 11 presents the SER of UFMC for $N = 1024$, $CP = 72$, $L_u = CP + 1 = 73$, 64-QAM, for HPA2 with $IBOs = 4, 3, 2\ dB$. We can confirm the good agreement between theoretical and simulation results.

Fig. 12 presents the SER of UFMC for $N = 1024$, 64-QAM, HPA2 with IBO= 4dB and various values of CP length (36, 72 and 144). When CP is increasing, the width of the holes in the time domain signal is increasing, corresponding to a lower equivalent IBO and thus a lower SER performance. We can see on Fig. 12 that, one more time, there is a good match between theoretical expressions and simulation results.

3) f-OFDM CASE

The theoretical SER for f-OFDM has the same expression as the SER of CP-OFDM except that coefficients K_0 and σ_d^2 are computed for the equivalent IBO_{equ}^{f-OFDM} given by 26.

Fig. 13 presents the SER of f-OFDM for $N = 1024$, $CP = 72$, $L_f = 512$, 64-QAM, for HPA2 with

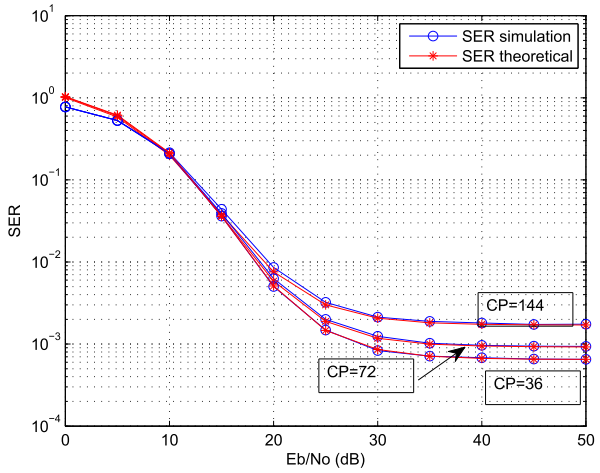

FIGURE 12. UFMC performance for different values of CP length, HPA2, IBO = 4dB, M = 1024, CP = [36, 72, 144].

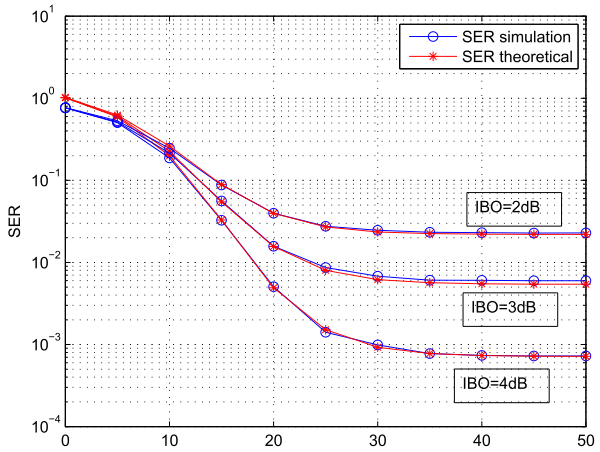

FIGURE 13. f-OFDM performance for HPA2 and IBO = 4, 3, 2dB.

$IBOs = 4, 3, 2\,dB$, the frame-length $K = 1$ and the number of active subcarriers is equal to $N.31/32 = 992$. Again, we can notice a very good match between theoretical expressions and simulation results.

Fig. 14 presents the SER of f-OFDM for $N = 1024$, HPA2 with IBO $= 5dB$, 64-QAM and various frame-lengths ($K = 1$ and 10). When K is decreasing, the distance between two holes, in the time domain signal, is decreasing, corresponding to a lower equivalent IBO and thus a lower SER performance. We can see on Fig. 14 that there is a good match between theoretical expressions and simulation results.

C. SER PERFORMANCE COMPARISON BETWEEN ALL THE MWFs AND HPA MODELS

Fig. 15 presents the SER of all the MWFs for the Rapp modified model HPA (HPA2) with an IBO equal to $4dB$ and a 64-QAM modulation. As stated previously in this section, FBMC/OQAM and OFDM have the same performance. WOLA-OFDM, UFMC and f-OFDM have lower performances than CP-OFDM as explained before.

Fig. 16 presents the SER of all the MWFs for the 3GPP model HPA (HPA1) with an IBO equal to $4dB$ and a 16-QAM

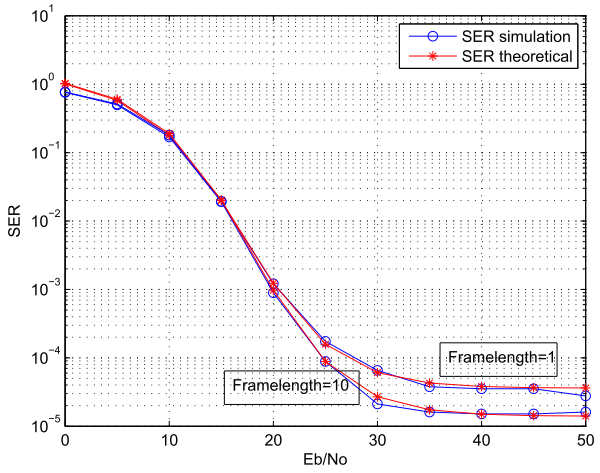

FIGURE 14. f-OFDM performance for different values of frame length ($K = 1$ and 10), HPA2, IBO = 5dB, M = 1024, CP = 72, $L_f = 512$.

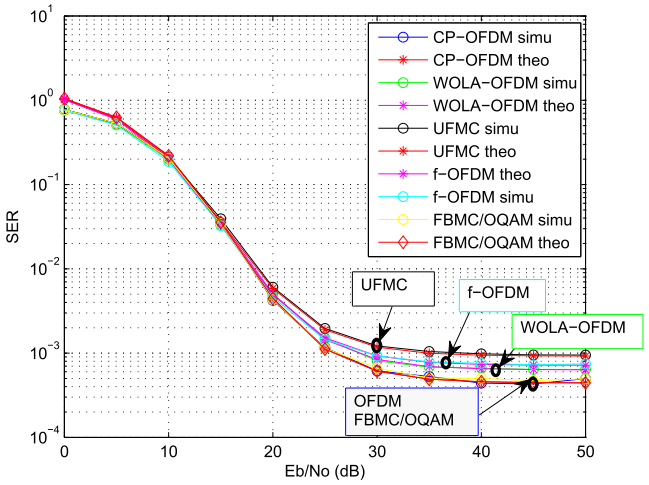

FIGURE 15. SER performance of all WFs for HPA2, IBO = 4dB, 64QAM.

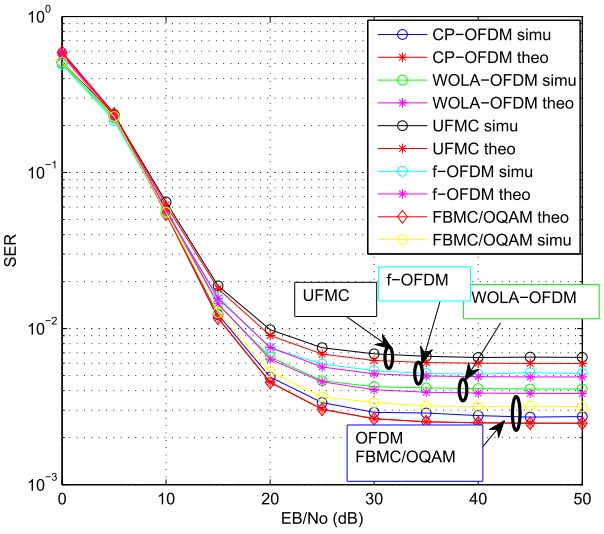

FIGURE 16. SER performance of all WFs for HPA1, IBO = 4dB, 16QAM.

modulation. We recall that this HPA model exhibits both AM/AM and AM/PM distortion. As in the case of HPA2, FBMC/OQAM and CP-OFDM show the same performance.

However WOLA-OFDM, UFMC and f-OFDM have lower performances than CP-OFDM.

V. CONCLUSION

Research, development and standardization activities for the 5G are in full action. As a fundamental component, the underlying post-OFDM waveform is expected to be able to support the coexistence of diverse services. In this paper, we provide details and explanation on the theoretical study of NLD on 5G and Beyond waveform candidates. In particular, we develop analytical expressions of SER to evaluate the effects of in-band NLD on CP-OFDM, WOLA-OFDM, UFMC, f-OFDM and BF-OFDM. Theoretical results validate the simulated ones and show that the AM/AM and AM/PM NLD affect strongly the performance of the studied WFs although their good properties in terms of reduced OOB emission. It is shown that these MWFs almost perform as the classical CP-OFDM when HPA is operated near its saturation region (e.g. where the energy efficiency is high). Based on these results, a higher attention must be paid for RF HPA effects that should be taken into account in the design of the beyond 5G MWFs for wireless communication systems.

REFERENCES

[1] S.-Y. Lien, S.-L. Shieh, Y. Huang, B. Su, Y.-L. Hsu, and H.-Y. Wei, "5G new radio: Waveform, frame structure, multiple access, and initial access," *IEEE Commun. Mag.*, vol. 55, no. 6, pp. 64–71, Jun. 2017.

[2] Y. Liu *et al.*, "Waveform design for 5G networks: Analysis and comparison," *IEEE Access*, vol. 5, pp. 19282–19292, 2017.

[3] M. Shafi *et al.*, "5G: A tutorial overview of standards, trials, challenges, deployment, and practice," *IEEE J. Sel. Areas Commun.*, vol. 35, no. 6, pp. 1201–1221, Jun. 2017.

[4] K. N. R. S. V. Prasad, E. Hossain, and V. K. Bhargava, "Energy efficiency in massive MIMO-based 5G networks: Opportunities and challenges," *IEEE Wireless Commun.*, vol. 24, no. 3, pp. 86–94, Jun. 2017.

[5] Y. Medjahdi *et al.*, "On the road to 5G: Comparative study of physical layer in MTC context," *IEEE Access*, vol. 5, pp. 26556–26581, 2017.

[6] M. J. Abdoli, M. Jia, and J. Ma, "Weighted circularly convolved filtering in OFDM/OQAM," in *Proc. IEEE 24th Annu. Int. Symp. Pers., Indoor, Mobile Radio Commun. (PIMRC)*, Sep. 2013, pp. 657–661.

[7] C. Kim, Y. H. Yun, K. Kim, and J.-Y. Seol, "Introduction to QAM-FBMC: From waveform optimization to system design," *IEEE Commun. Mag.*, vol. 54, no. 11, pp. 66–73, Nov. 2016.

[8] H. Lin and P. Siohan, "Multi-carrier modulation analysis and WCP-COQAM proposal," *EURASIP J. Adv. Signal Process.*, vol. 2014, p. 79, May 2014.

[9] C. Lélé, P. Siohan, and R. Legouable, "The alamouti scheme with CDMA-OFDM/OQAM," *EURASIP J. Adv. Signal Process.*, vol. 2010, 2010. [Online]. Available: https://dblp.org/rec/bib/journals/ejasp/LeleSL10. doi: 10.1155/2010/703513.

[10] Y. Medjahdi, M. Terré, D. Le Ruyet, D. Roviras, and A. Dziri, "Performance analysis in the downlink of asynchronous OFDM/FBMC based multi-cellular networks," *IEEE Trans. Wireless Commun.*, vol. 10, no. 8, pp. 2630–2639, Aug. 2011.

[11] R. Zayani, Y. Medjahdi, H. Shaiek, and D. Roviras, "WOLA-OFDM: A potential candidate for asynchronous 5G," in *Proc. IEEE Global Commun. Conf. (GLOBECOM)*, Dec. 2016, pp. 1–5.

[12] R. Gerzaguet, Y. Medjahdi, D. Demmer, R. Zayani, J. B. Doré, H. Shaiek, and D. Roviras, "Comparison of promising candidate waveforms for 5G: WOLA-OFDM versus BF-OFDM," in *Proc. Int. Symp. Wireless Commun. Syst. (ISWCS)*, Aug. 2017, pp. 355–359.

[13] H. Bouhadda, H. Shaiek, D. Roviras, R. Zayani, Y. Medjahdi, and R. Bouallegue, "Theoretical analysis of BER performance of nonlinearly amplified FBMC/OQAM and OFDM signals," *EURASIP J. Adv. Signal Process.*, vol. 2014, p. 60, 2014. [Online]. Available: https://dblp.org/rec/bib/journals/ejasp/BouhaddaSRZMB14. doi: 10.1186/1687-6180-2014-60.

[14] P. Guan *et al.*, "5G field trials: OFDM-based waveforms and mixed numerologies," *IEEE J. Sel. Areas Commun.*, vol. 35, no. 6, pp. 1234–1243, Jun. 2017.

[15] *R1-162199: Waveform Candidates*, Qualcomm, San Diego, CA, USA, 2016.

[16] V. Vakilian, T. Wild, F. Schaich, S. ten Brink, and J. F. Frigon, "Universal-filtered multi-carrier technique for wireless systems beyond LTE," in *Proc. IEEE Globecom Workshops (GC Wkshps)*, Dec. 2013, pp. 223–228.

[17] F. Schaich and T. Wild, "Waveform contenders for 5G—OFDM vs. FBMC vs. UFMC," in *Proc. 6th Int. Symp. Commun., Control Signal Process. (ISCCSP)*, May 2014, pp. 457–460.

[18] T. Wild, F. Schaich, and Y. Chen, "5G air interface design based on universal filtered (UF-)OFDM," in *Proc. 19th Int. Conf. Digit. Signal Process.*, Aug. 2014, pp. 699–704.

[19] J. Abdoli, M. Jia, and J. Ma, "Filtered OFDM: A new waveform for future wireless systems," in *Proc. IEEE 16th Int. Workshop Signal Process. Adv. Wireless Commun. (SPAWC)*, Jun. 2015, pp. 66–70.

[20] M. Bellanger, "FBMC physical layer: A primer," ICT-PHYDYAS, Tech. Rep., Jun. 2010, pp. 1–31. [Online]. Available: http://www.ictphydyas.org/teamspace/internal-folder/FBMC-Primer_06-2010.pdf

[21] B. Farhang-Boroujeny, "OFDM versus filter bank multicarrier," *IEEE Signal Process. Mag.*, vol. 28, no. 3, pp. 92–112, May 2011.

[22] G. Zhou and R. Raich, "Spectral analysis of polynomial nonlinearity with applications to RF power amplifiers," *EURASIP J. Appl. Signal Process.*, vol. 2004, no. 256395, pp. 1840–1931, 2004.

[23] J. K. Vuolevi, T. Rahkonen, and J. P. A. Manninen, "Measurement technique for characterizing memory effects in RF power amplifiers," *IEEE Trans. Microw. Theory Techn.*, vol. 49, no. 8, pp. 1380–1383, Aug. 2001.

[24] W. Bosch and G. Gatti, "Measurement and simulation of memory effects in predistortion linearizers," *IEEE Trans. Microw. Theory Techn.*, vol. 37, no. 12, pp. 1885–1890, Dec. 1989.

[25] J. Kim and K. Konstantinou, "Digital predistortion of wideband signals based on power amplifier model with memorys," *Electron. Lett.*, vol. 37, no. 23, pp. 1417–1418, 2001.

[26] K. Hyunchul and J. Kenney, "Behavioral modeling of nonlinear RF power amplifiers considering memory effects," *IEEE Trans. Microw. Theory Techn.*, vol. 51, no. 12, pp. 2495–2504, Dec. 2003.

[27] *RP-160671: Study on New Radio Access Technology*, NTT DOCOMO, Inc, Tokyo, Japan, 2016.

[28] P. Colantonio, F. Giannini, and E. Limiti, *High Efficiency RF and Microwave Solid State Power Amplifiers*. London, U.K.: Wiley, 2009.

[29] P. N. Landin and D. Rönnow, "RF PA modeling considering odd-even and odd order polynomials," in *Proc. IEEE Symp. Commun. Veh. Technol. Benelux (ISCVT)*, Nov. 2015, pp. 1–6.

[30] R. Raich, H. Qian, and G. T. Zhou, "Orthogonal polynomials for power amplifier modeling and predistorter design," *IEEE Trans. Veh. Technol.*, vol. 53, no. 5, pp. 1468–1479, Sep. 2004.

[31] C. Rapp, "Effects of HPA nonlinearity on 4-DPSK-OFDM signal for digital sound broadcasting systems," in *Proc. 2nd Eur. Conf. Satellite Commun.*, Oct. 1991, pp. 38–45.

[32] A. A. M. Saleh, "Frequency-independent and frequency-dependent nonlinear models of TWT amplifiers," *IEEE Trans. Commun.*, vol. COMM-29, no. 11, pp. 1715–1720, Nov. 1981.

[33] *Realistic Power Amplifier Model for the New Radio Evaluation*, document R4-163314, 3GPP TSG-RAN WG4 Meeting, 3GPP, 2016.

[34] D. Dardari, V. Tralli, and A. Vaccari, "A theoretical characterization of nonlinear distortion effects in OFDM systems," *IEEE Trans. Commun.*, vol. 48, no. 10, pp. 1755–1764, Oct. 2000.

[35] M. C. Dakhli, R. Zayani, O. B. Belkacem, and R. Bouallegue, "Theoretical analysis and compensation for the joint effects of HPA nonlinearity and RF crosstalk in VBLAST MIMO-OFDM systems over Rayleigh fading channel," *EURASIP J. Wireless Commun. Netw.*, vol. 2014, p. 61, Apr. 2014.

[36] A. Ligata, H. Gacanin, and T. Javornik, "On performance of MIMO-OFDM/TDM using MMSE-FDE with nonlinear HPA in a multipath fading channel," *IEICE Trans. Commun.*, vol. E97, no. 9, pp. 1947–1957, 2014.

[37] J. Bussgang, *Crosscorrelation Functions of Amplitude-Distorted Gaussian Signals*. Cambridge, MA, USA: MIT Press, 1952.

[38] J. Proakis, *Digital Communications*. New York, NY, USA: McGraw-Hill, 2008.

HMAIED SHAIEK received the Engineering degree from the National Engineering School of Tunis, in 2002, the master's degree from the Université de Bretagne Occidentale, in 2003, and the Ph.D. degree from the Lab-STICC CNRS Team, Telecom Bretagne, in 2007. He was with Canon Inc., until 2009. He left the industry to integrate with the École Nationale d'Ingénieurs de Brest, as a Lecturer, from 2009 to 2010. In 2011, he joined the Conservatoire National des Arts et Métiers as an Associate Professor in electronics and signal processing. He holds three patents, and has authored or co-authored ten journal papers and over 35 conference papers. His research interests include performance analysis of multicarrier modulations with nonlinear power amplifiers, PAPR reduction, and power amplifier linearization. He contributed to the FP7 EMPHATIC European project and is involved in two national projects, such as Accent5 and Wong5, funded by the French National Research Agency.

RAFIK ZAYANI received the Engineering, M.Sc., and Ph.D. degrees from the École Nationale d'Ingénieurs de Tunis (ENIT), in 2003, 2004, and 2009, respectively, where he was with the Laboratory of Communications Systems, from 2003 to 2005. Since 2005, he has been with the Innov'COM Laboratory, Sup'Com School, Tunisia. From 2004 to 2009, he was with the Department of Telecommunication and Networking, Institut Supérieur d'Informatique (ISI), Tunis, as a Contractual Assistant Professor. Since 2009, he has been an Associate Professor (tenure position) with ISI, Tunisia. Since 2010, he has been an Associate Researcher with the CEDRIC Laboratory, Conservatoire National des Arts et Métiers, France. He is an Established Researcher with long experience in multicarrier communications and energy efficiency enhancement by transmitter linearization techniques (baseband DPD) and PAPR reduction; high power amplifier characterization; neural networks; identification modeling and equalization; and MIMO technologies. He was involved in enhanced multicarrier waveforms, such as FBMC-OQAM, UFMC, GFDM, BF-OFDM, and WOLA-OFDM. He has contributed to several European (EMPHATIC) and French (WONG5) projects that aim at designing flexible air-interfaces for future wireless communications (5G and Beyond). He has recently been awarded the H2020 Marie Sklodowska-Curie Actions (MSCA) Individual Fellowship Grant for his ADMA5 project proposal.

YAHIA MEDJAHDI received the degree in engineering from the École Nationale Polytechnique of Algiers, Algeria, the M.Sc. degree in signal processing for communications from the Institute Galilée, Paris 13 University, in 2008, and the Ph.D. degree from the Conservatoire National des Arts et Métiers (CNAM), in 2012. He was a Researcher with the CEDRIC Laboratory, CNAM, an Assistant Professor with Khemis-Miliana University, Algeria, and a Post doctoral Researcher with the ICTEAM Laboratory, Université Catholique de Louvain, Belgium. He is currently an Assistant Professor with the Institut Supérieur d'Électronique de Paris. He has been involved in several ICT-European and French projects, such as PHYDYAS, EMPHATIC, and WONG5, dealing with waveform design for 5G and PMR systems. He has authored or co-authored 30 papers in peer-reviewed journals and international conferences and one book chapter. His research interests include flexible multicarrier waveform design, cooperative communications, PAPR reduction, and non-linearity of power amplifiers.

DANIEL ROVIRAS was born in 1958. He received the Engineering degree from SUPÉLEC, Paris, France, in 1981, and the Ph.D. degree from the National Polytechnic Institute of Toulouse, Toulouse, France, in 1989. He spent in the industry as a Research Engineer for seven years. He joined the Electronics Laboratory, École Nationale Supérieure d'Électrotechnique, d'Électronique, d'Informatique, et des Télécommunications (ENSEEIHT). In 1992, he joined the Engineering School, ENSEEIHT, as an Assistant Professor, where he has been a Full Professor, since 1999. Since 2008, he has been a Professor with the Conservatoire National des Arts et Métiers (CNAM), Paris, where his teaching activities are related to radio-communication systems. He is currently a member of the CEDRIC Laboratory, CNAM. His research activity was first centered around transmission systems based on infrared links. Since 1992, his topics have been widened to more general communication systems, such as mobile and satellite communications systems, equalization, predistortion of nonlinear amplifiers, and multicarrier systems.